Low-Dose MDCT of Patients With Spinal Instrumentation Using Sparse Sampling: Impact on Metal Artifacts

Nico Sollmann, MD, PhD[1,2], Kai Mei, PhD[3,4], Isabelle Riederer, MD[1], Simon Schön, MD[1], Jan S. Kirschke, MD[1,2], Bernhard Meyer, MD[5], Claus Zimmer, MD[1], Thomas Baum, MD[1], Peter B. Noël, PhD[3,4]

Musculoskeletal Imaging · Original Research

Keywords

artifacts, image enhancement, MDCT, postoperative complications, spine

Submitted: Mar 4, 2020
Revision requested: Apr 10, 2020
Revision received: May 6, 2020
Accepted: May 26, 2020
First published online: Mar 11, 2021

The authors declare that they have no disclosures relevant to the subject matter of this article.

Supported by the University of Pennsylvania Research Foundation; the Deutsche Forschungsgemeinschaft (432290010) to J. S. Kirschke, T. Baum, and P. B. Noël; the Dr.-Ing. Leonhard Lorenz-Stiftung Foundation (project 968/19) and B. Braun Foundation (project BBST-D-19-00106) to N. Sollmann; and Philips Healthcare.

OBJECTIVE. The purpose of our study was to evaluate simulated sparse-sampled MDCT combined with statistical iterative reconstruction (SIR) for low-dose imaging of patients with spinal instrumentation.

MATERIALS AND METHODS. Thirty-eight patients with implanted hardware after spinal instrumentation (24 patients with short- or long-term instrumentation-related complications [i.e., adjacent segment disease, screw loosening or implant failure, or postoperative hematoma or seroma] and 14 control subjects with no complications) underwent MDCT. Scans were simulated as if they were performed with 50% (P50), 25% (P25), 10% (P10), and 5% (P5) of the projections of the original acquisition using an in-house–developed SIR algorithm for advanced image reconstructions. Two readers performed qualitative image evaluations of overall image quality and artifacts, image contrast, inspection of the spinal canal, and diagnostic confidence (1 = high, 2 = medium, and 3 = low confidence).

RESULTS. Although overall image quality decreased and artifacts increased with reductions in the number of projections, all complications were detected by both readers when 100% of the projections of the original acquisition (P100), P50, and P25 imaging data were used. For P25 data, diagnostic confidence was still high (mean score ± SD: reader 1, 1.2 ± 0.4; reader 2, 1.3 ± 0.5), and interreader agreement was substantial to almost perfect (weighted Cohen κ = 0.787–0.855). The mean volumetric CT dose index was 3.2 mGy for P25 data in comparison with 12.6 mGy for the original acquisition (P100 data).

CONCLUSION. The use of sparse sampling and SIR for low-dose MDCT in patients with spinal instrumentation facilitated considerable reductions in radiation exposure. The use of P25 data with SIR resulted in no missed complications related to spinal instrumentation and allowed high diagnostic confidence, so using only 25% of the projections is probably enough for accurate and confident diagnostic detection of major instrumentation-related complications.

Lower back pain has a high prevalence and is one of the top reasons for seeking medical advice. Depending on the distinct medical diagnosis, surgical intervention must often be considered; spinal instrumentation ranks among the most frequently performed procedures and has shown considerable increases in case numbers over the past decades [1–3]. Spinal instrumentation is performed for various clinical indications, such as for the correction of scoliosis [4, 5]; stabilization of pseudospondylolisthesis [6, 7]; surgical treatment of degenerative disk disease [8, 9]; or stabilization of osteoporotic, pathologic, or traumatic vertebral fractures [10–12].

Hardware implanted for spinal instrumentation commonly consists of pairs of pedicle screws and interconnecting rods made of stainless steel [13, 14]. Postoperative or long-term complications of this hardware include hematoma or seroma, infections, adjacent segment disease (ASD), implant failure, faulty placement, or screw loosening, all of which have been shown to be closely associated with patient morbidity and to possibly require revision surgery [15, 16]. Hence, the goal of imaging must be the early detection of these complications.

[1]Department of Diagnostic and Interventional Neuroradiology, School of Medicine, Klinikum rechts der Isar, Technical University of Munich, Ismaninger Strasse 22, 81675 Munich, Germany. Address correspondence to N. Sollmann (Nico.Sollmann@tum.de).

[2]TUM-Neuroimaging Center, Klinikum rechts der Isar, Technical University of Munich, Munich, Germany.

[3]Department of Diagnostic and Interventional Radiology, School of Medicine, Klinikum rechts der Isar, Technical University of Munich, Munich, Germany.

[4]Department of Radiology, Perelman School of Medicine, University of Pennsylvania, Philadelphia, PA.

[5]Department of Neurosurgery, School of Medicine, Klinikum rechts der Isar, Technical University of Munich, Munich, Germany.

doi.org/10.2214/AJR.20.23083

AJR 2021; 216:1308–1317

ISSN-L 0361–803X/21/2165–1308

CT plays a key role in diagnosing complications immediately after surgery or during follow-up because of its wide availability, robustness, high contrast between bony structures and soft tissue, and high spatial resolution [13, 17–19]. In particular, CT is frequently preferred over MRI because the presence of metallic hardware at the spine, often spanning multiple vertebral levels, causes image distortion during acquisition that often is too severe to allow sufficient diagnostic image evaluation. However, using CT in patients treated with spinal instrumentation has relevant shortcomings. First, metal artifacts due to the implanted hardware can also affect image quality and diagnostic confidence of CT because metallic hardware causes beam-hardening and photon starvation of the x-ray [17, 20]. Second, CT generally comes at the cost of radiation exposure to the patient, which may entail relevant estimated cancer risk ratios that need to be considered with regard to patient safety [21, 22]. It is remarkable that, despite the high use of imaging in daily clinical routine, these issues remain largely unsolved for conventional MDCT.

Although advanced CT systems, such as dual-layer or spectral CT, have shown potential to facilitate metal artifact reduction, they are less widely distributed than MDCT units [23–26]. Furthermore, image reconstruction algorithms with artifact suppression have been made commercially available, but these algorithms are still not optimal because they may introduce new artifacts and compromises, making further advancements necessary [27–31].

Reductions of radiation exposure without clinically relevant restrictions in diagnostic quality for MDCT might be achieved by targeted modifications of image acquisition schemes (e.g., reduction in tube current or the use of sparse sampling) in combination with applications of advanced image reconstruction algorithms. Because the common approach of tube current reduction inherently leads to considerable increases in image noise, which can—particularly in combination with additional implant-related metal artifacts—severely impede diagnostic evaluation of images, sparse sampling might reflect a novel promising alternative. Sparse sampling refers to the acquisition of fewer projection images during scanning, which results in maintained energy delivery for the individual projection image but lower overall radiation exposure because of the decreased number of projections [32, 33]. Thus, preserved image quality for the individual projection can be achieved while circumventing the influence of electronic readout noise [32, 33]. When combined with an advanced image reconstruction, such as statistical iterative reconstruction (SIR), image noise might be further suppressed while structural image information can be preserved to a level still allowing diagnostics [32, 34, 35]. However, to our knowledge, sparse-sampled MDCT combined with SIR has not been applied to spine imaging in patients with spinal instrumentation.

We hypothesized that sparse-sampled MDCT combined with SIR would enable clear reductions in radiation exposure while delivering images of sufficient diagnostic quality in patients treated with spinal instrumentation.

Materials and Methods

Design and Inclusion

This retrospective study was approved by the local institutional review board and was conducted in accordance with the Declaration of Helsinki. The criteria for inclusion in this study were the following: hardware implanted during spinal instrumentation; unenhanced MDCT examination of the spine performed in our department (Department of Diagnostic and Interventional Neuroradiology, Klinikum rechts der Isar, Technical University of Munich) irrespective of the suspected diagnosis, clinical symptoms, or clinical indication for imaging; and an FOV capturing at least the adjacent segments to the levels of spinal instrumentation. Exclusion criteria were age of less than 18 years; motion artifacts in imaging data; vertebral fractures or malignant bone lesions in the FOV above or below the instrumented levels (to dedicatedly focus on instrumentation-related complications); and other implants in the FOV besides hardware related to the spinal instrumentation.

We searched the PACS at Klinikum rechts der Isar for patients fulfilling these criteria. The inclusion period for this study was March to May 2019. Overall, 38 patients were included in this study.

MDCT

Scanning was performed in a routine clinical setting using a standard MDCT scanner (Ingenuity Core 128, Philips Healthcare) with the patients placed in a supine position. An initial scout scan was obtained for planning the FOV, which was placed to cover the implanted hardware and the adjacent vertebral levels in all patients. Diagnostic imaging was then performed by helical scanning with the tube current modulated implicitly by the MDCT system. The volumetric CT dose index ($CTDI_{vol}$) was obtained from the scanning summaries that are automatically documented by the scanner. Table 1 shows the scanning parameters and details for the MDCT examinations.

Sparse Sampling and Statistical Iterative Reconstruction

The raw imaging data of the helical examinations were exported directly from the MDCT system and used for simulations of sparse-sampled imaging combined with an in-house–developed SIR algorithm. Sparse sampling was applied at levels of 100% (P100), 50% (P50), 25% (P25), 10% (P10), and 5% (P5) of the original projection data, which was achieved by reading every second, fourth, 10th, and 20th projection angle and deleting the remaining projections in the sinogram [36–39]. The number of sampled projections per full rotation was reduced, but other parameters such as tube voltage, x-ray intensity, patient location, and projection geometry were not changed.

A total-variation approach was used to efficiently reduce image noise ($\lambda = 0.01$ and $n = 50$) [40, 41]. Regarding the image reconstruction, SIR was performed with ordered-subset–separable paraboloidal surrogation and a momentum-based accelerating approach [38, 42–45]. In this regard, the likelihood term for the reconstruction was generated with log-converted projection data considering a Gaussian noise model.

In addition, we applied regularization to compensate for the effects of undersampled projections and to improve the convergence of the iterative reconstruction algorithm. The regularization term was based on a Huber penalty, and its distinct strength was chosen in consensus by two board-certified radiologists with 7 years (reader 1) and 6 years (reader 2) of experience in radiology. The aim during selection of the specific regularization strength was to sufficiently depress image noise while preserving adequate bone and soft-tissue contrast at the same time. The

TABLE 1: Scanning and Image Reconstruction Parameters

Parameter	Value
Tube voltage (kV)	
Mean ± SD	134.7 ± 8.8
Range	120–140
Tube current (mA)	
Mean ± SD	287.6 ± 56.3
Range	192–397
Rotation time (s)	
Mean ± SD	0.61 ± 0.15
Range	0.4–1.0
Exposure (mAs)	
Mean ± SD	148.2 ± 51.1
Range	69.0–258.0
Volumetric CT dose index (mGy)	
Mean ± SD	12.6 ± 4.3
Range	6.5–23.0
FOV (mm)	200 × 200
Slice thickness (mm)	0.9
Voxel spacing (mm^3)	0.39 × 0.39 × 0.9
Reformations	Sagittal, axial, coronal
Window settings (HU)[a]	
Window width[b]	2500
Window center[b]	500

[a]The window settings were individually adjustable.
[b]Standard bone window settings were used as the default settings.

same strength of regularization was used for all simulated data using sparse sampling (i.e., all P100, P50, P25, P10, and P5 data). Using the air and water information from the calibration data in the MDCT scanner, voxel intensities (linear attenuation coefficients) were translated into attenuations in Hounsfield units. Table 1 shows reconstruction details for sparse-sampled imaging.

Image Evaluation

The sparse-sampled image data reconstructed with SIR were transferred to a PACS (IDS7, Sectra) for qualitative evaluation by readers 1 and 2. The readers assessed overall image quality, overall artifacts, image contrast, and inspection of the spinal canal using Likert scales (Table 2). Furthermore, they noted the presence and type of any complication of spinal instrumentation, such as screw loosening or implant failure (Figs. 1 and 2), ASD (Fig. 3), and hematoma or seroma (Fig. 4), and rated their subjective diagnostic confidence (Table 2).

Both readers independently evaluated the sparse-sampled image data with SIR of all patients after patient pseudonymization using the PACS viewer. They were blinded to the ratings of each other and the clinical patient data as well as the radiology reports created during clinical routine for the original MDCT data reconstructed with standard algorithms and used for clinical diagnostic purposes. However, they were informed about the clinical indications for MDCT that were provided by the treating neurosurgeons. Readers started with the evaluations of P100 data of all patients followed by an assessment of P50, P25, P10, and P5 data with an interval of at least 2 weeks between the readings of data with different numbers of projections. The order of presentation of patient cases was subject to randomization during every round of image readings.

Statistics

GraphPad Prism (version 6.0, GraphPad Software) and SPSS for Microsoft Windows (version 25.0, IBM) were used for statistical data analyses. A p value of $< .05$ was considered statistically significant.

Descriptive statistics were calculated for patient-related characteristics including demographics, the scores assigned by each reader, and the number and entities of complications related to spinal instrumentation. For comparisons of scores assigned for overall image quality, overall artifacts, image contrast, inspection of the spinal canal, and diagnostic confidence of P100 data and data with fewer projections, Wilcoxon signed-rank tests were conducted for the evaluations of both readers (i.e., P100 vs P50, P25, P10, and P5 for reader 1 and reader 2, respectively).

The weighted Cohen kappa was calculated between the scores of the two readers regarding the single items of image evaluation to assess interreader agreement. The following scale for interpre-

TABLE 2: Likert Scores for Qualitative Image Evaluation and Assessment of Diagnostic Confidence

	Score				
Item	1	2	3	4	5
Qualitative image evaluation					
Overall image quality	Very good to perfect quality	Good to very good quality	Medium quality	Poor quality	Inappropriate quality
Overall artifacts	No artifacts	Minimal artifacts	Prominent artifacts	Major artifacts	Severe artifacts
Image contrast	Very good to perfect contrast	Good to very good contrast	Medium contrast	Poor contrast	Inappropriate contrast
Inspection of the spinal canal	Good visibility of spinal canal	Moderate visibility of spinal canal	Poor visibility of spinal canal		
Diagnostic confidence					
Confidence	High confidence	Medium confidence	Low confidence		

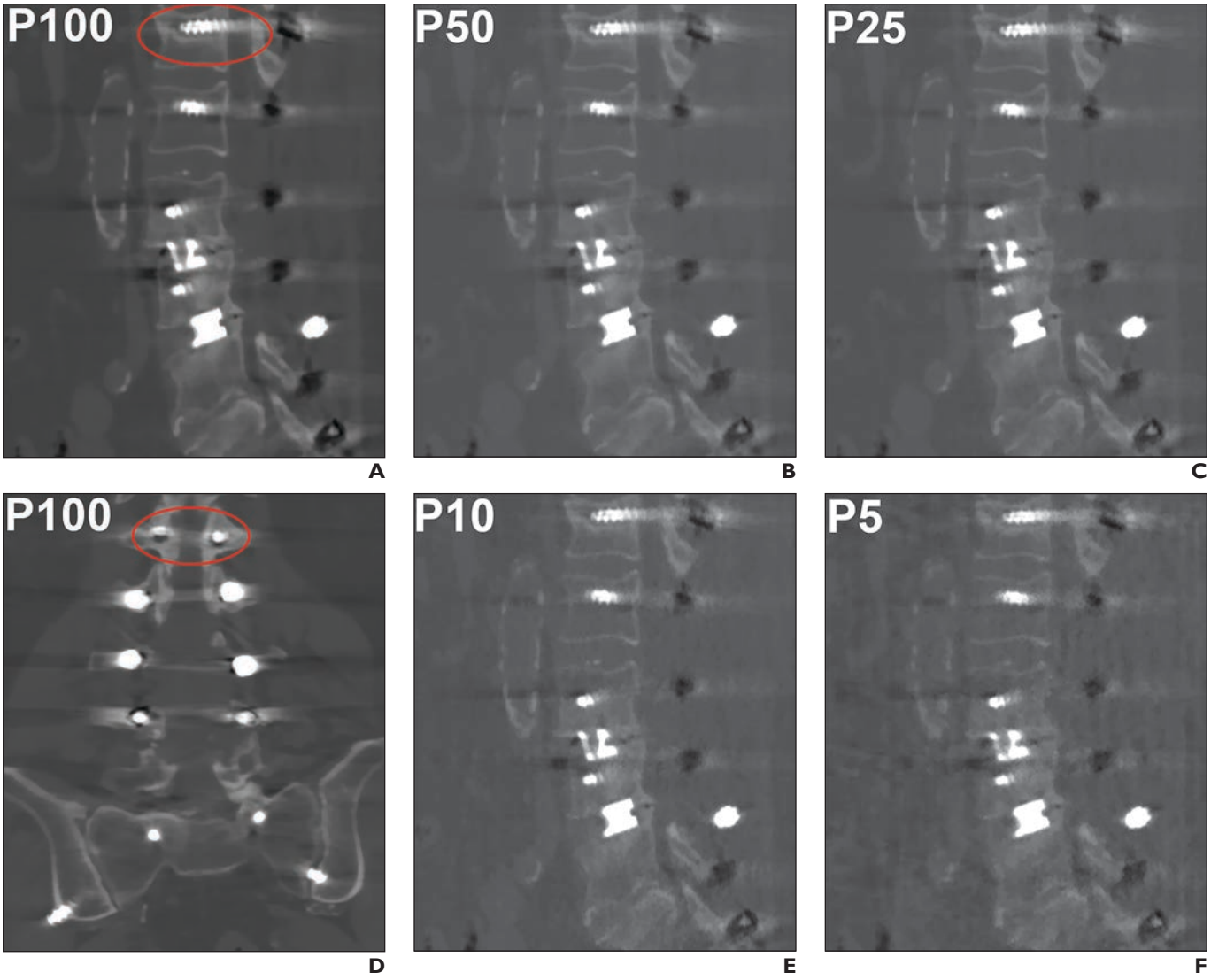

Fig. 1—71-year-old man with screw loosening. Patient had undergone dorsal stabilization (L1 to ilium with intervertebral cages for L3–L4 and L4–L5) 1.5 years earlier. This figure presents case with screw loosening at level L1 (both sides).
A–F, Sagittal (**A–C**), coronal (**D**), and sagittal (**E** and **F**) MDCT images with statistical iterative reconstruction are shown for MDCT with full number of projections (100%) (P100) and for sparse-sampled MDCT using 50% (P50), 25% (P25), 10% (P10), and 5% (P5) of original projections. Red ovals in **A** and **D** mark area of screw loosening.

tation of kappa values was considered: a kappa value of less than 0, no agreement; 0–0.20, slight agreement; 0.21–0.40, fair agreement; 0.41–0.60, moderate agreement; 0.61–0.80, substantial agreement; and 0.81–1, almost-perfect agreement.

Results

Cohort Characteristics

Of the 38 patients included in this study, 24 patients (63.2%) showed complications related to spinal instrumentation (screw loosening or implant failure, ASD, or hematoma or seroma) according to the clinical radiologic reports. Three patients (7.9%) showed more than one of these complications. The mean interval between the last spine surgery and MDCT for this study group was 1.7 ± 3.3 (SD) years (range, postoperative day 1–14.8 years). Detailed patient-related characteristics are displayed in Table 3.

The mean $CTDI_{vol}$ of the original-dose MDCT examination with the full number of projections (P100) was 12.6 mGy. The $CTDI_{vol}$ of the sparse-sampled imaging data accounted for 6.3 mGy (P50), 3.2 mGy (P25), 1.3 mGy (P10), and 0.6 mGy (P5) of the mean $CTDI_{vol}$ of the P100 examination.

Image Evaluation

Overall image quality—Overall image quality decreased with the reductions of projections according to the scores of both readers. In comparison with P100 data, all sparse-sampled image data showed statistically significantly higher scores ($p < .05$; Table 4). Although images of P100 and P50 were determined to be of good to excellent quality, P25 data showed only medium quality and P10 and P5 data were of poor and inappropriate quality, respectively. Interreader comparison, as expressed by

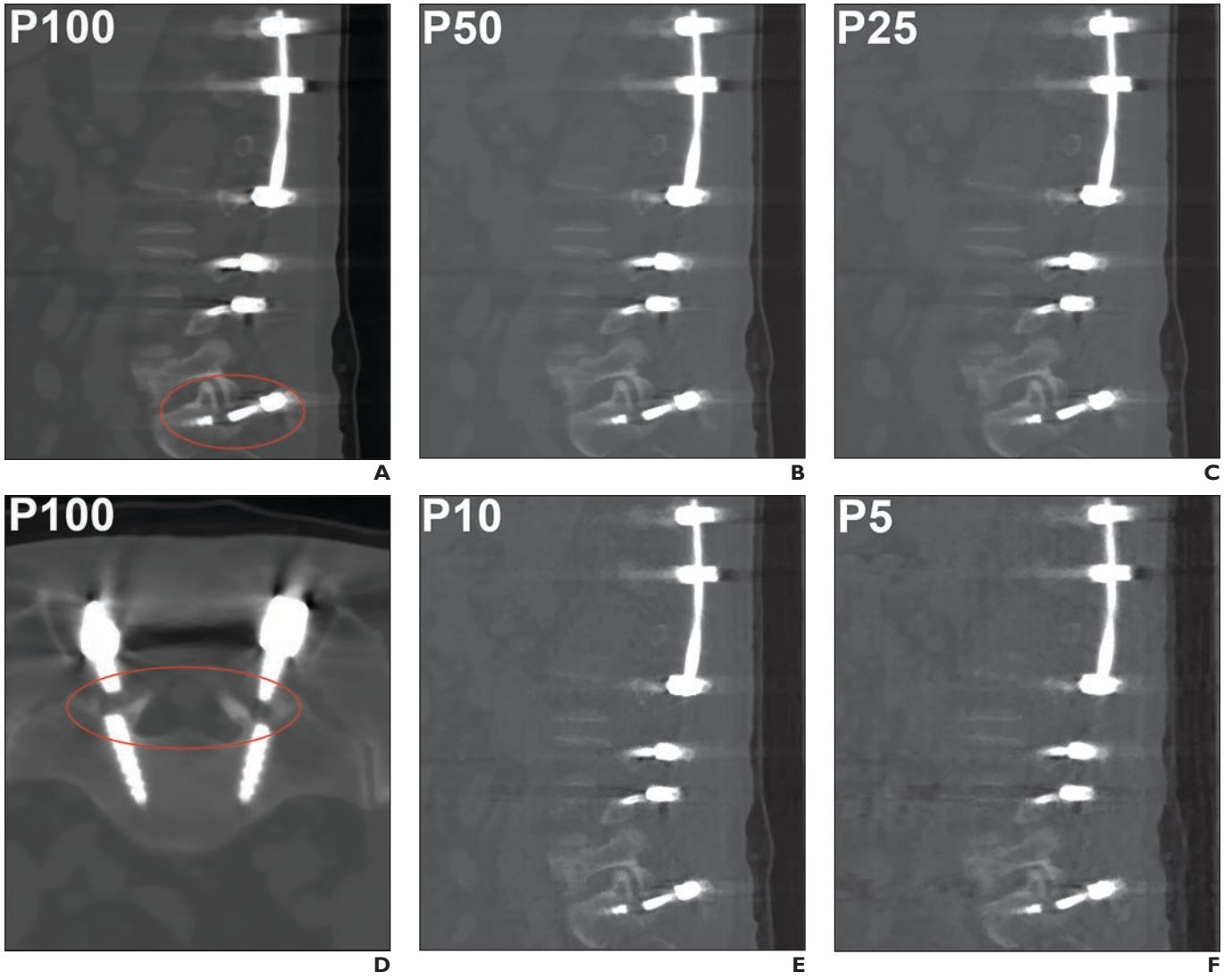

Fig. 2—56-year-old man with implant failure. Patient had undergone dorsal stabilization (T11–S1) 3.5 years earlier. This figure presents case of implant failure at level S1 (both sides) in context of previously performed dorsal stabilization.
A–F, Sagittal (**A–C**), axial (**D**), and sagittal (**E** and **F**) MDCT images with statistical iterative reconstruction are shown for MDCT with full number of projections (100%) (P100) and for sparse-sampled MDCT using 50% (P50), 25% (P25), 10% (P10), and 5% (P5) of original projections. Red ovals in **A** and **D** mark site of implant failure.

weighted Cohen kappa values, was in the range of substantial to almost-perfect agreement for P100 to P10 data (κ = 0.704–0.822) and was moderate for P5 data (κ = 0.522; Table 4).

Overall artifacts—There was an increase in overall artifacts with reductions of projections, and differences between sparse-sampled image data and data with the full number of projections (P100) were statistically significant ($p < .05$; Table 4). Images of P100 appeared with only minimal artifacts, whereas P50 and P25 data showed prominent artifacts; P10 data, major artifacts; and P5 data, severe artifacts. Interreader agreement was substantial to almost perfect for P100 to P10 data (κ = 0.685–0.956) and was moderate for P5 data (κ = 0.453; Table 4).

Image contrast—Image contrast decreased with reductions of projections, and the differences between data with the full number of projections (P100) and sparse-sampled image data were statistically significant for all levels of sparse sampling ($p < .05$; Table 4). Image contrast was scored as good to excellent for P100 and P50 data, medium for P25 data, poor for P10 data, and inappropriate for P5 data. Substantial to almost-perfect agreement was observed between scores of both readers for all data except P5 data (P100 to P10, κ = 0.704–0.896; P5, κ = 0.305; Table 4).

Inspection of the spinal canal—The visibility of the spinal canal was good to moderate for P100 to P10 data, whereas it was poor for P5 data. The comparison of scores for the inspection of the spinal canal between images of P100 data and all levels of sparse-sampled data showed statistically significant differences ($p < .05$; Table 4). Interreader agreement was substantial to almost perfect for all data (P100 to P10, κ = 0.609–0.894) except P5 data, which showed moderate agreement (κ = 0.529; Table 4).

Detection of complications and diagnostic confidence—All complications related to spinal instrumentation (i.e., screw loosening or implant failure, ASD, and hematoma or seroma) were correctly

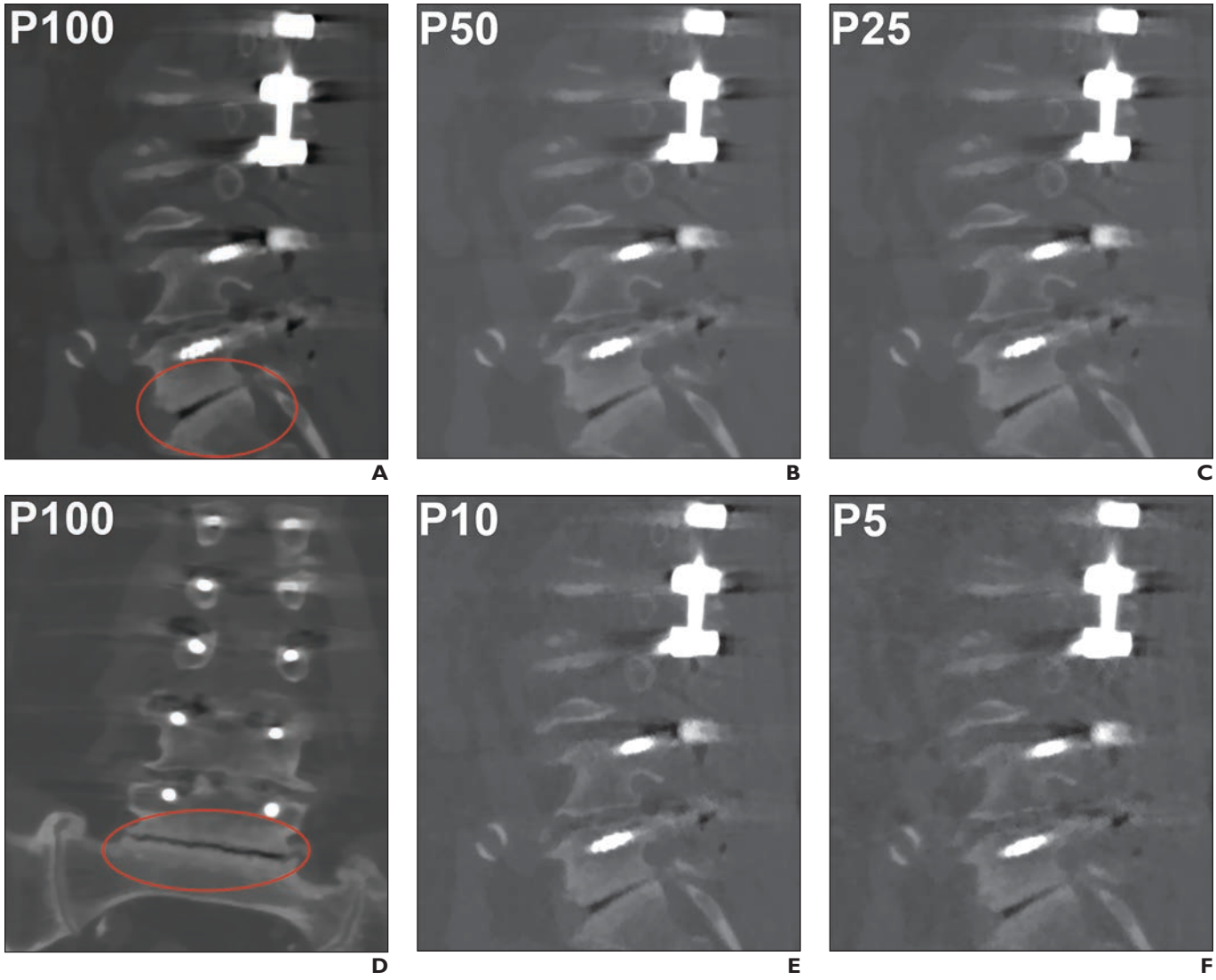

Fig. 3—72-year-old man with adjacent segment disease (ASD). Patient had undergone dorsal stabilization (L1–L5) 6.5 years earlier. This figure presents patient with ASD at segment L5–S1 due to dorsal stabilization.
A–F, Sagittal (**A–C**), coronal (**D**), and sagittal (**E** and **F**) MDCT images with statistical iterative reconstruction for MDCT with full number of projections (100%) (P100) and sparse-sampled MDCT using 50% (P50), 25% (P25), 10% (P10), and 5% (P5) of original projections. Red ovals in **A** and **D** mark area of ASD.

detected in patients without any missed complications for P100, P50, and P25 data according to the evaluations of both readers (Figs. 1–4). In the P10 data, two complications were not detected by reader 1, and one complication was missed by reader 2. Furthermore, for the P5 data, nine and 11 complications were not detected by reader 1 and reader 2, respectively.

High diagnostic confidence was observed according to mean scores (± SD) of both readers for P100 (reader 1, 1.1 ± 0.3; reader 2, 1.1 ± 0.2), P50 (reader 1, 1.1 ± 0.3; reader 2, 1.1 ± 0.3), and P25 (reader 1, 1.2 ± 0.4; reader 2, 1.3 ± 0.5) imaging data (Fig. 5). For P10 data, diagnostic confidence was medium (reader 1, 1.8 ± 0.5; reader 2, 1.9 ± 0.5), and diagnostic confidence was scored as low for P5 data (reader 1, 2.6 ± 0.5; reader 2, 2.7 ± 0.5; Fig. 5). Statistically significant differences were observed between data with the full number of projections (P100) and P25, P10, and P5 data for scores of both readers, respectively ($p < .05$). Interreader agreement was substantial to almost perfect for all data except P5 data (P100 to P10, $\kappa = 0.787–0.855$; P5, $\kappa = 0.467$).

Discussion

This study investigated sparse sampling combined with SIR for MDCT of patients with spinal instrumentation. Although overall image quality and contrast decreased and artifacts increased with the reductions of the numbers of projections, diagnostic confidence for the detection of common postoperative or follow-up complications related to spinal instrumentation remained high for reductions down to 25% of the original projections. Moreover, for image data with 25% of the original projections (P25), no complication was missed.

Hardware implanted for spinal instrumentation mostly consists of metal components, which predispose to metal artifacts that can profoundly affect image quality and diagnostic confi-

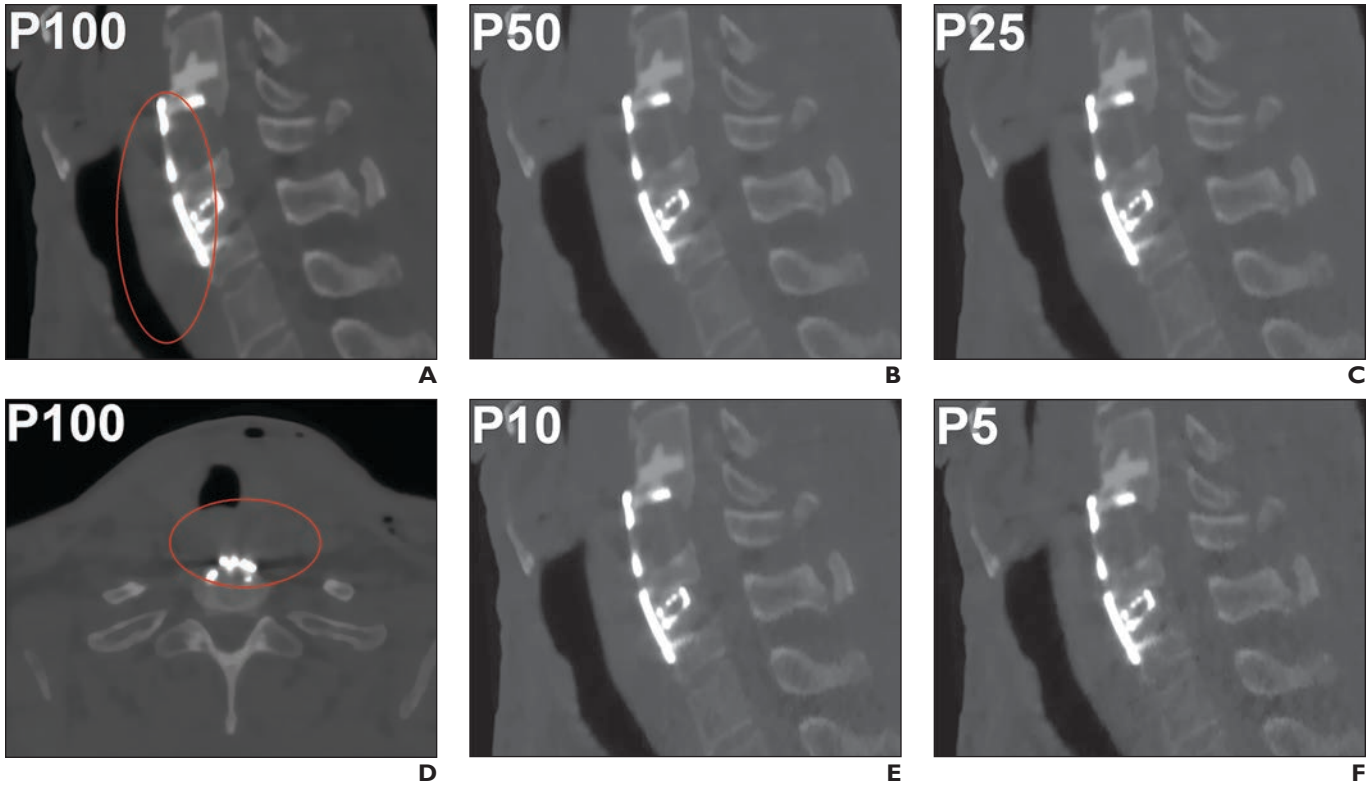

Fig. 4—50-year-old man with hematoma. Patient had undergone ventral stabilization (C5–T1 with intervertebral cages for C6–C7 and C7–T1) 3 days earlier. This figure presents patient with postoperative hematoma in prevertebral space at level of cervical spine 3 days after ventral stabilization.
A–F, Sagittal (**A–C**), axial (**D**), and sagittal (**E** and **F**) MDCT images with statistical iterative reconstruction for MDCT with full number of projections (100%) (P100) and for sparse-sampled MDCT using 50% (P50), 25% (P25), 10% (P10), and 5% (P5) of original projections. Red ovals in **A** and **D** mark area of hematoma.

dence for x-ray–based imaging modalities. Metallic hardware causes beam-hardening and photon starvation of the x-ray, which commonly result in dark bands on images that are referred to as streak artifacts [17, 20]. These artifacts impede clear depiction of the implanted hardware, structures in the vicinity of the hardware, and metal-bone interfaces [17, 20]. Thus, patients with implanted metallic hardware are challenging to image when it comes to artifact reductions and lowering of radiation exposure because merely decreasing the tube current—an approach conventionally used to reduce radiation exposure for MDCT—is likely to fail. A decrease in tube current is likely to fail because the reduced energy applied inherently leads to considerable increases in image noise, making metal artifacts even more prominent and restricting the diagnostic usability of data. A fundamentally different way to reduce radiation exposure is to acquire fewer projection images, which is referred to as sparse sampling [32, 33]. The anticipated benefit of sparse sampling over tube current reduction is reflected by better maintenance of image quality while circumventing the influence of noise [32, 33]. Therefore, this approach seems ideally suited for application in patients with spinal instrumentation.

Sparse sampling is a novel technique that has recently been applied to MDCT of the spine for different purposes [36, 37]. A recent study was able to show that assessment of vertebral bone mineral density and of microstructure parameters using sparse-sampled MDCT is more robust than MDCT with ultra-low tube currents [36]. Furthermore, sparse-sampled MDCT provided adequate image quality and diagnostic accuracy for vertebral fracture detection with only 50% of the original projections, in contrast to MDCT with tube currents lowered by 50% [37]. However, sparse sampling has not yet been applied to patients with implanted hardware at the

TABLE 3: Patient, Procedure, and Hardware Characteristics

Characteristic	Value
Age (y), median (range)	71.3 (32.1–90.7)
Sex, % of patients	
Men	76.3
Women	23.7
No. of vertebrae in FOV, median (range)	8.0 (3–23)
Area covered by FOV, % of patients	
Cervical spine	31.6
Thoracic spine	65.8
Lumbosacral spine	68.4
Type of stabilization, % of patients	
Dorsal	92.1
Ventral	5.3
Combined dorsal and ventral	2.6

(Table 3 continues on next page)

TABLE 3: Patient, Procedure, and Hardware Characteristics (continued)

Characteristic	Value
No. of fused segments, median (range)	3.0 (1–8)
No. of screws per side, median (range)	4.0 (2–8)
Cement augmentation, % of patients	15.8
Intervertebral body cages, % of patients	36.8
Vertebral body replacement, % of patients	23.7
Complications related to spinal instrumentation, % of patients	
None	36.8
Screw loosening or implant failure	34.2
ASD	7.9
Hematoma or seroma	13.2
Screw loosening or implant failure and ASD	5.3
Screw loosening or implant failure and hematoma or seroma	2.6

Note—ASD = adjacent segment disease.

spine to our knowledge. Our results show that sparse-sampled MDCT data with only 25% of the initial projections combined with SIR is capable of providing images that can be used for adequate diagnostics of complications of spinal instrumentation with preserved high diagnostic confidence.

Improvement of image quality and, thus, diagnostic usability of MDCT data can also be facilitated by application of advanced image reconstruction algorithms [32, 34, 35]. This study used an in-house–developed SIR algorithm; however, reconstruction solutions for metal artifact reduction are commercially available [27]. The use of common commercially available image reconstruction algorithms with metal artifact reduction may harbor the risk of introducing new, uncommon artifacts and image compromises [28–31]. These unintentionally produced artifacts can include perihardware or pedicle screw lucency and abnormal intraosseous cement distribution that can interfere with correct diagnostics in patients with spinal instrumentation [31]. Hence, further development of reconstruction algorithms particularly in patients with spinal instrumentation is welcomed to avoid misdiagnosis and, in the worst case, unnecessary treatment related to erroneous detection of instrumentation-related complications. Using both beneficial image acquisition combined with advanced reconstruction, such as sparse sampling with SIR, may further reduce artifacts in imaging data of patients with implanted hardware.

Imaging using CT comes at the cost of radiation exposure to the patient: one-time scanning with a modern scanner applies an estimated effective dose of 5.6 and 10.0 mSv for the lumbar and whole dorsal spine, respectively, thus potentially entailing a relevant estimated cancer risk ratio for the individual patient [21, 22]. In this regard, the linear no-threshold (LNT) model implies a uniform cancer risk per unit dose from higher to lower doses and assumes there is no threshold dose for radiation-induced cancer [46, 47]. Thus, in terms of the LNT model that is considered the currently accepted standard concept for radiation protection, any dose reduction is welcomed and would be directly related to a reduced risk of cancer induction and to increased patient safety. Wide acceptance of the LNT model is related to its

TABLE 4: Qualitative Image Evaluation

Qualitative Image Evaluation	P100	P50	*p*	P25	*p*	P10	*p*	P5	*p*
Overall image quality									
Reader 1	2.2 ± 0.7	2.4 ± 0.6	**.005**	2.9 ± 0.7	**< .001**	3.7 ± 0.7	**< .001**	4.7 ± 0.5	**< .001**
Reader 2	2.2 ± 0.9	2.5 ± 0.9	**.001**	2.8 ± 0.8	**< .001**	3.8 ± 0.8	**< .001**	4.5 ± 0.6	**< .001**
κ	0.792	0.704	—	0.822	—	0.782	—	0.522	—
Overall artifacts									
Reader 1	2.4 ± 0.6	2.7 ± 0.6	**.003**	3.3 ± 0.6	**< .001**	4.1 ± 0.6	**< .001**	4.8 ± 0.4	**< .001**
Reader 2	2.5 ± 0.6	2.7 ± 0.7	**.004**	3.4 ± 0.7	**< .001**	4.1 ± 0.7	**< .001**	4.8 ± 0.4	**< .001**
κ	0.956	0.803	—	0.685	—	0.799	—	0.453	—
Image contrast									
Reader 1	1.9 ± 0.7	2.2 ± 0.6	**< .001**	3.0 ± 0.7	**< .001**	3.7 ± 0.7	**< .001**	4.8 ± 0.4	**< .001**
Reader 2	1.8 ± 0.7	2.3 ± 0.7	**< .001**	2.9 ± 0.7	**< .001**	3.7 ± 0.8	**< .001**	4.6 ± 0.5	**< .001**
κ	0.896	0.721	—	0.787	—	0.704	—	0.305	—
Inspection of spinal canal									
Reader 1	1.5 ± 0.5	1.6 ± 0.5	**.01**	1.9 ± 0.3	**< .001**	2.5 ± 0.5	**< .001**	2.9 ± 0.3	**< .001**
Reader 2	1.5 ± 0.5	1.6 ± 0.5	**.03**	1.8 ± 0.4	**< .001**	2.4 ± 0.6	**< .001**	2.9 ± 0.3	**< .001**
κ	0.894	0.728	—	0.685	—	0.609	—	0.529	—

Note—Evaluation was performed for sparse-sampled scans derived from MDCT using the full number of projections (100%) (P100) combined with statistical iterative reconstruction (SIR) as well as for scans simulated as if they were performed with 50% (P50), 25% (P25), 10% (P10), and 5% (P5) of original projections and also reconstructed with SIR. Scores are given as mean ± SD, and interreader agreement is expressed by weighted Cohen kappa values; *p* values refer to the comparisons of respective sparse-sampled scans to scans with 100% of projections and SIR. Boldface shows statistically significant values ($p < .05$). Dash (—) indicates not applicable.

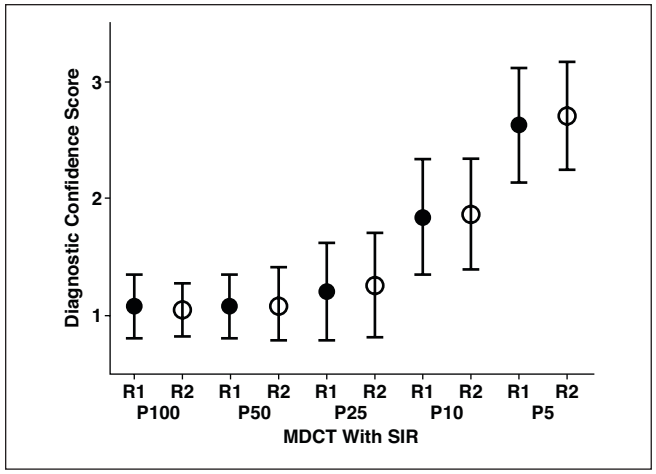

Fig. 5—Plot shows diagnostic confidence scores of reader 1 (R1) and reader 2 (R2) for MDCT with 100% of projections (P100) and statistical iterative reconstruction (SIR) as well as for sparse-sampled MDCT using 50% (P50), 25% (P25), 10% (P10), and 5% (P5) of projections of original acquisition and SIR. Scores are shown as mean (*circles*) ± 1 SD (*whiskers*).

good fit to data from several observational studies on radiation exposure and cancer development and the lack of a reasonably competitive alternative model [48]. However, the LNT model can be seen as controversial, which might particularly hold true for diagnostic imaging studies with inherently limited radiation exposure [47, 48]. For the current study, using only 25% of the initial projections would lower the $CTDI_{vol}$ to 3.2 mGy versus 12.6 mGy as estimated for imaging with the full number of projections for our patient cohort. The exact numbers may be subject to variations depending on the size of the FOV and the specific MDCT scanner used, among other factors, but they may point toward the high potential of sparse-sampled MDCT for patient safety. Although the distinct evaluation of a potentially reduced cancer risk attributable to decreased radiation exposure is out of the scope of the current study, the achievement of lowered exposure would fit to the implications of the LNT model and the prominent ALARA principle [46, 49].

Our study has limitations that must be considered. First, sparse sampling has not been made commercially available yet, but prototypes already exist and may find their way to the clinical setting. Second, this study did not compare imaging data of sparse-sampled MDCT with SIR to routine MDCT images using commercially available image reconstruction algorithms with metal artifact suppression because of the current impossibility to transfer the simulated data back to the MDCT system. Thus, direct evaluation of potential superiority of the presented approach to commercially available solutions could not be performed. Third, we used MDCT because this technique is most widely distributed and is applied frequently in centers dealing with patients with spinal instrumentation. Acquisitions with dual-layer or spectral CT have shown considerable potential to facilitate metal artifact reduction [23–26]. However, neither dual-layer CT nor spectral CT is broadly available, and the respective systems are expensive. Thus, further development of MDCT for imaging of patients with implanted hardware still appears highly important for clinical routine, and a combination of techniques should be sought in the future.

Conclusion

This study is the first to investigate sparse sampling combined with SIR for MDCT of patients with spinal instrumentation. Using the presented approach can enable considerable reductions in radiation exposure. The use of P25 data with SIR resulted in no missed complications related to spinal instrumentation and allowed high diagnostic confidence, so using only 25% of the projections is probably enough for accurate and confident diagnostic detection of major instrumentation-related complications.

References

1. Rajaee SS, Bae HW, Kanim LE, Delamarter RB. Spinal fusion in the United States: analysis of trends from 1998 to 2008. *Spine* 2012; 37:67–76
2. Martin BI, Mirza SK, Spina N, Spiker WR, Lawrence B, Brodke DS. Trends in lumbar fusion procedure rates and associated hospital costs for degenerative spinal diseases in the United States, 2004 to 2015. *Spine* 2019; 44:369–376
3. Grotle M, Småstuen MC, Fjeld O, et al. Lumbar spine surgery across 15 years: trends, complications and reoperations in a longitudinal observational study from Norway. *BMJ Open* 2019; 9:e028743
4. Rose PS, Lenke LG. Classification of operative adolescent idiopathic scoliosis: treatment guidelines. *Orthop Clin North Am* 2007; 38:521–529, vi
5. Sucato DJ. Management of severe spinal deformity: scoliosis and kyphosis. *Spine* 2010; 35:2186–2192
6. Wood KB, Fritzell P, Dettori JR, Hashimoto R, Lund T, Shaffrey C. Effectiveness of spinal fusion versus structured rehabilitation in chronic low back pain patients with and without isthmic spondylolisthesis: a systematic review. *Spine* 2011; 36(suppl):S110–S119
7. Weinstein JN, Lurie JD, Tosteson TD, et al. Surgical versus nonsurgical treatment for lumbar degenerative spondylolisthesis. *N Engl J Med* 2007; 356:2257–2270
8. Hioki A, Miyamoto K, Kodama H, et al. Two-level posterior lumbar interbody fusion for degenerative disc disease: improved clinical outcome with restoration of lumbar lordosis. *Spine J* 2005; 5:600–607
9. Phillips FM, Slosar PJ, Youssef JA, Andersson G, Papatheofanis F. Lumbar spine fusion for chronic low back pain due to degenerative disc disease: a systematic review. *Spine* 2013; 38:E409–E422
10. Mikles MR, Stchur RP, Graziano GP. Posterior instrumentation for thoracolumbar fractures. *J Am Acad Orthop Surg* 2004; 12:424–435
11. Tomita K, Kawahara N, Kobayashi T, Yoshida A, Murakami H, Akamaru T. Surgical strategy for spinal metastases. *Spine* 2001; 26:298–306
12. Ponnusamy KE, Iyer S, Gupta G, Khanna AJ. Instrumentation of the osteoporotic spine: biomechanical and clinical considerations. *Spine J* 2011; 11:54–63
13. Rutherford EE, Tarplett LJ, Davies EM, Harley JM, King LJ. Lumbar spine fusion and stabilization: hardware, techniques, and imaging appearances. *RadioGraphics* 2007; 27:1737–1749
14. Slone RM, MacMillan M, Montgomery WJ, Heare M. Spinal fixation. Part 2. Fixation techniques and hardware for the thoracic and lumbosacral spine. *RadioGraphics* 1993; 13:521–543
15. Slone RM, MacMillan M, Montgomery WJ. Spinal fixation. Part 3. Complications of spinal instrumentation. *RadioGraphics* 1993; 13:797–816
16. Young PM, Berquist TH, Bancroft LW, Peterson JJ. Complications of spinal instrumentation. *RadioGraphics* 2007; 27:775–789
17. Douglas-Akinwande AC, Buckwalter KA, Rydberg J, Rankin JL, Choplin RH. Multichannel CT: evaluating the spine in postoperative patients with orthopedic hardware. *RadioGraphics* 2006; 26(suppl 1):S97–S110
18. Ha AS, Petscavage-Thomas JM. Imaging of current spinal hardware: lumbar spine. *AJR* 2014; 203:573–581

19. Patel VV, Andersson GB, Garfin SR, Resnick DL, Block JE. Utilization of CT scanning associated with complex spine surgery. *BMC Musculoskelet Disord* 2017; 18:52
20. Barrett JF, Keat N. Artifacts in CT: recognition and avoidance. *RadioGraphics* 2004; 24:1679–1691
21. Richards PJ, George J. Diagnostic CT radiation and cancer induction. *Skeletal Radiol* 2010; 39:421–424
22. Richards PJ, George J, Metelko M, Brown M. Spine computed tomography doses and cancer induction. *Spine* 2010; 35:430–433
23. Dangelmaier J, Schwaiger BJ, Gersing AS, et al. Dual layer computed tomography: reduction of metal artefacts from posterior spinal fusion using virtual monoenergetic imaging. *Eur J Radiol* 2018; 105:195–203
24. Guggenberger R, Winklhofer S, Osterhoff G, et al. Metallic artefact reduction with monoenergetic dual-energy CT: systematic ex vivo evaluation of posterior spinal fusion implants from various vendors and different spine levels. *Eur Radiol* 2012; 22:2357–2364
25. Große Hokamp N, Neuhaus V, Abdullayev N, et al. Reduction of artifacts caused by orthopedic hardware in the spine in spectral detector CT examinations using virtual monoenergetic image reconstructions and metal-artifact-reduction algorithms. *Skeletal Radiol* 2018; 47:195–201
26. Neuhaus V, Große Hokamp N, Abdullayev N, et al. Metal artifact reduction by dual-layer computed tomography using virtual monoenergetic images. *Eur J Radiol* 2017; 93:143–148
27. Wellenberg RHH, Hakvoort ET, Slump CH, Boomsma MF, Maas M, Streekstra GJ. Metal artifact reduction techniques in musculoskeletal CT-imaging. *Eur J Radiol* 2018; 107:60–69
28. Huang JY, Kerns JR, Nute JL, et al. An evaluation of three commercially available metal artifact reduction methods for CT imaging. *Phys Med Biol* 2015; 60:1047–1067
29. Jeong S, Kim SH, Hwang EJ, Shin CI, Han JK, Choi BI. Usefulness of a metal artifact reduction algorithm for orthopedic implants in abdominal CT: phantom and clinical study results. *AJR* 2015; 204:307–317
30. Kotsenas AL, Michalak GJ, DeLone DR, et al. CT metal artifact reduction in the spine: can an iterative reconstruction technique improve visualization? *Am J Neuroradiol* 2015; 36:2184–2190
31. Wayer DR, Kim NY, Otto BJ, Grayev AM, Kuner AD. Unintended consequences: review of new artifacts introduced by iterative reconstruction CT metal artifact reduction in spine imaging. *Am J Neuroradiol* 2019; 40:1973–1975
32. Willemink MJ, Noël PB. The evolution of image reconstruction for CT: from filtered back projection to artificial intelligence. *Eur Radiol* 2019; 29:2185–2195
33. Abbas S, Lee T, Shin S, Lee R, Cho S. Effects of sparse sampling schemes on image quality in low-dose CT. *Med Phys* 2013; 40:111915
34. Willemink MJ, de Jong PA, Leiner T, et al. Iterative reconstruction techniques for computed tomography. Part 1. Technical principles. *Eur Radiol* 2013; 23:1623–1631
35. Willemink MJ, Leiner T, de Jong PA, et al. Iterative reconstruction techniques for computed tomography. Part 2. Initial results in dose reduction and image quality. *Eur Radiol* 2013; 23:1632–1642
36. Mei K, Kopp FK, Bippus R, et al. Is multidetector CT-based bone mineral density and quantitative bone microstructure assessment at the spine still feasible using ultra-low tube current and sparse sampling? *Eur Radiol* 2017; 27:5261–5271
37. Sollmann N, Mei K, Hedderich DM, et al. Multi-detector CT imaging: impact of virtual tube current reduction and sparse sampling on detection of vertebral fractures. *Eur Radiol* 2019; 29:3606–3616
38. Sollmann N, Mei K, Schwaiger BJ, et al. Effects of virtual tube current reduction and sparse sampling on MDCT-based femoral BMD measurements. *Osteoporos Int* 2018; 29:2685–2692
39. Zhao Z, Gang GJ, Siewerdsen JH. Noise, sampling, and the number of projections in cone-beam CT with a flat-panel detector. *Med Phys* 2014; 41:061909
40. Rudin LI, Osher S, Fatemi E. Nonlinear total variation based noise removal algorithms. *Physica D* 1992; 60:259–268
41. Chan TF, Shen J. *Image processing and analysis: variational, PDE, wavelet, and stochastic methods*. Society for Industrial and Applied Mathematics, 2005
42. Fessler JA. Statistical image reconstruction methods for transmission tomography. In: Fitzpatrick JM, Sonka M, eds. *Handbook of medical imaging,* vol. 2. *Medical image processing and analysis*. SPIE Publications, 2000:1–70
43. Kim D, Ramani S, Fessler JA. Combining ordered subsets and momentum for accelerated X-ray CT image reconstruction. *IEEE Trans Med Imaging* 2015; 34:167–178
44. Sollmann N, Mei K, Schön S, et al. Systematic evaluation of low-dose MDCT for planning purposes of lumbosacral periradicular infiltrations. *Clin Neuroradiol* 2020; 30:749–759
45. Sollmann N, Mei K, Riederer I, et al. Tube current reduction in CT angiography: how low can we go in imaging of patients with suspected acute stroke? *AJR* 2019; 213:410–416
46. Shamoun DY. Linear no-threshold model and standards for protection against radiation. *Regul Toxicol Pharmacol* 2016; 77:49–53
47. Weber W, Zanzonico P. The controversial linear no-threshold model. *J Nucl Med* 2017; 58:7–8
48. Siegel JA, Welsh JS. Does imaging technology cause cancer? Debunking the linear no-threshold model of radiation carcinogenesis. *Technol Cancer Res Treat* 2016; 15:249–256
49. Prasad KN, Cole WC, Haase GM. Radiation protection in humans: extending the concept of as low as reasonably achievable (ALARA) from dose to biological damage. *Br J Radiol* 2004; 77:97–99